ISSN 1349-1113
JAXA-RR-04-013E

JAXA Research and Development Report

Numerical Study on the Lateral Jet Flow of Helicopter Rotor: Part 1. Tip Vortex of Fixed Blades

Choongmo YANG, Takashi AOYAMA, Shigeru SAITO, and Jehyun BAEK

August 2004

Japan Aerospace Exploration Agency

CONTENTS

Numerical Study on the Lateral Jet Flow of Helicopter Rotor: Part 1. Tip Vortex of Fixed Blades*

ヘリコプタロータの翼端噴射に関する数値解析：第1部 固定ブレードの翼端渦*

Choongmo YANG*1, Takashi AOYAMA*1, Shigeru SAITO*1, and Jehyun BAEK*2

梁忠模*1、青山剛史*1、齊藤茂*1、Jehyun BAEK*2

ABSTRACT

Blade vortex interaction noise (BVI), which is generated by an impulsive change in the pressure distribution over the interacting blade preceding the pressure jump, propagates sound to far field observers. In general, these interactions occur in forward-descent flight conditions, especially during a landing approach. The acoustic signal from BVI is generally in the frequency range to which the human subjective response is most sensitive. In order to reduce BVI noise, many researchers have been studying not only passive remedies such as rotor tip design and leading edge modification, but also active devices such as a higher harmonic control method, active tabs, flap and tip-jet blowing.

The National Aerospace Laboratory (NAL) in Japan and Pohang University of Science and Technology (POSTECH) in Korea have conducted a collaborative research program on the effects of lateral wing-tip blowing to reduce BVI noise from helicopter rotors. The lateral wing-tip method is one of the active control methods to control the generation and behavior of tip vortical flow by blowing a jet flow at the tip of the main rotor. In the first stage of the research, three-dimensional compressible Euler/Navier-Stokes equations are solved to calculate the effect of blowing air from the blade tip on the tip vortex of a fixed single blade. In the next stage, predictions of BVI noise will be made by combining an unsteady Euler code with an aeroacoustic code based on the Ffowcs-Williams and Hawkings formulation.

The present report corresponds to the first part of this effort: determining the effect of blowing air from the blade tip on the tip vortex of a fixed single blade. The computed circumferential velocity profiles of the tip vortex are compared with experimental results with a single fixed wing to validate the numerical technique. The numerical results include the position of the vortex center along the vortical flow, the size and strength of the rolled tip vortex, and the circulation and maximum tangential velocity of the tip vortex under various jet conditions. Jet flow from the wing tip can diffuse the tip vortex such as producing larger core sizes and lower velocity gradients, which can be effective ways to reduce BVI noise from a rotary wing.

Key Words: Blade Vortex Interaction (BVI), CFD, Euler Equation, Navier-Stokes Equation, Helicopter, Tip vortex

* received 26 August, 2004(H16 年 8 月 26 日受付)

*1 Japan Aerospace Exploration Agency（宇宙航空研究開発機構）

*2 Pohang University of Science and Technology, KOREA(浦項工科大学校, 韓国)

概　　要

ブレード／渦干渉（Blade-Vortex Interaction: BVI）騒音は、先行するメイン・ロータのブレードが吐き出した翼端渦が後続ブレードの翼端付近を通過する時に起こる弱い干渉、あるいは先行ブレードの翼端渦を後続ブレードが切る時に起こる強い干渉によって、ブレードの空力荷重が急激に変動することから発生する。この騒音は、特に前進方向の下方に指向性を持ち、主にヘリコプタが着陸する際に発生するため、付近の住民に与える影響が大きく、都市部におけるヘリポート設置の妨げとなっている。BVI 騒音の低減法としては、翼型や翼端形状を工夫する受動的なものから、高調波制御、アクティブ・フラップ、翼端噴射などの能動的なものまで、様々な方法が提案されている。

航空宇宙技術研究所（NAL）と韓国の浦項工科大学校（POSTECH）は、能動的な BVI 騒音低減法の中で、特に翼端噴射に着目して、その低減効果を CFD で解析することを目的に、共同研究を行った。この翼端噴射とは、ヘリコプタ・ブレードの翼端から半径方向外向きにジェットを噴き出すことで、翼端渦の位置や構造を変化（渦の循環を弱めたりコア半径を大きくする）させ、BVI 騒音を低減しようとする技術である。本研究では、まず、単一格子を用いて固定ブレードの翼端噴射が翼端渦の挙動に及ぼす影響を Euler/Navier-Stokes コードで解析した。続いて、移動重合格子法を用いた３次元非定常 Euler コードと Ffowcs Williams and Hawkings (FW-H) の式に基づく空力音響コードを組み合わせた計算法によって、回転場での翼端噴射の騒音低減効果を解析した。

本報告は、前者の固定ブレードの結果について述べるものである。ここで用いたコードの検証は、実験値との比較を通して行った。解析の具体的な目的は、翼端噴射速度、噴射方向、噴射口面積をパラメトリックに変化させたとき、それが翼端渦の挙動（翼端渦の大きさ、中心位置、循環、最大周速度など）に及ぼす影響を把握することである。結果として、翼端噴射は渦のコア半径を大きくして翼端渦の拡散を促すとともに、その位置を翼端面内から外側に移動させることが分かった。これは、翼端噴射を回転ブレードに適用したとき、BVI 騒音を低減する可能性を示唆するものである。

1. INTRODUCTION

1.1 Various noises in helicopter

There are several kinds of noise sources in helicopter as shown in Figure 1.1. Among these noises, rotor noises including main-rotor and tail-rotor, are of interest in the fields of aerodynamics and aeroacoustics.

Helicopter rotor noises can be divided into 4 kinds of noise mechanisms as shown in Figure 1.2[1]. One is discrete loading noise due to steady and azimuthally dependent blade loading, which dominates the lower harmonics of the blade passage frequency. Next is discrete impulsive noise, or Blade Vortex Interaction (BVI) noise which is already well-known to dominate a large number of harmonics. Broadband noise of Blade Wake Interaction (BWI) is dominant at somewhat higher frequencies because of BWI from blade interaction with turbulence in and about the general rotor wake. The last one is broadband self-noise due to blade interaction with boundary layer and near-wake turbulence, which controls the high-frequency part of spectra. [2-5]

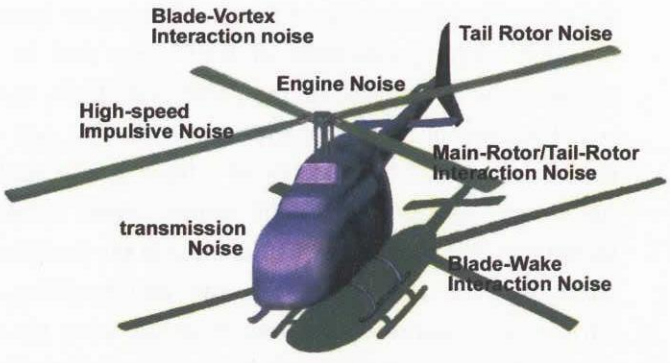

Figure 1.1 Several noises in helicopter

The relative significance of each of these mechanisms is dependent on rotor operating conditions. Blade Vortex Interaction (BVI) is dominant during forward-decent flight, which is most important to human sensitivity. Blade-Wake-Interaction (BWI) is known to be significant in level or climb flight in the mid-frequency range. At high climb angles, BWI is reduced and self-noise from blade boundary-layer turbulence becomes the most prominent.

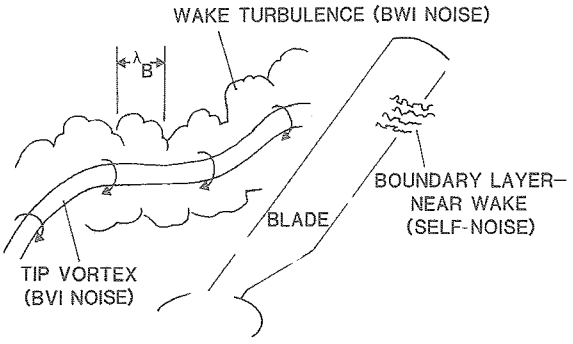

Figure 1.2 Diagram of noise sources in helicopter rotor

An example of typical waveform of noise spectrum from microphone in Figure 1.3[1] shows dominant regions for four individual source mechanisms. Compared to other noises, BVI generates critically high noise depending on flight conditions.

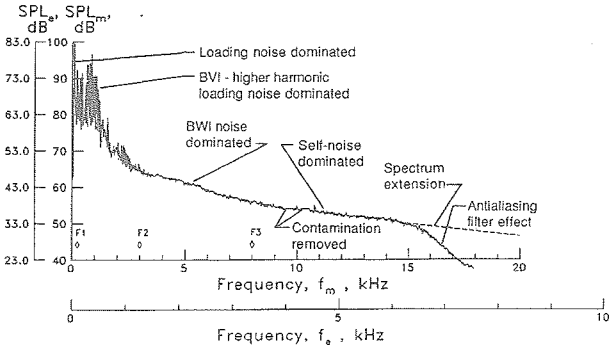

Figure 1.3 Wave forms of noise in helicopter

The aerodynamics and acoustics of BVI have been examined both analytically and experimentally up to now, and many researches have been conducted to reduce or control BVI noise[6-9]. Several methods which couple aerodynamic and aeroacoustic codes have been developed to predict the BVI noise by the Aero-Flight-dynamics Directorate (AFDD) of the U.S.Army[10], DLR of Germany[11], ONERA of France[12], and ATIC of Japan, respectively[13]. Tadghighi et al. [14] developed a procedure for BVI noise prediction, based on a coupling among a lifting-line code (to provide the vortex wake geometry), a three-dimensional unsteady full-potential code (to provide blade surface pressure), and an acoustic code using Farassat's 1A of the Ffowcs Williams and Hawking (FW-H) formulation. Several research groups have been also developing prediction code using various combinations of analytical codes to obtain wake geometry, airload or blade surface pressure, and acoustic signature. Yu et al.[15] summarized the comparisons of the analytical results for Operational Loads Survey (OLS) model rotor. The activity of the BVI working group by Caradonna et al.[16] was also reported, and their work provided a plenty of progress in the helicopter noise research.

BVI is function of many geometrical and aerodynamic parameters, such ad hover-tip speed, advance ratio, wake geometry, vortex strength and core size, miss distance, blade deformations, intersection angle and so on. The intensity of the BVI noise is strongly affected by the factors, 1) the local strength of the tip vortex, 2) the core size of the tip vortex, 3) the local interaction angle between the blade an vortex line, and 4) the miss-distance between the vortex and the blade. Each research has approached to one of these parameters to reduce BVI noise.

Passive devices have been considered to suppress high noise levels by rotor tip design and leading edge modification. Many researchers have been trying to modify the blade-tip planform to limit shock-wave generation and stall occurrence on the advancing rotor blade.[17,18] Active devices in BVI noise have been employed such as Individual Blade Control (IBC)[19] method, Higher Harmonic Control (HHC)[20] method and Tailing Edge Flap (TEF)[21] method. These methods are concerned with changing miss distance by disturbing blade or tip vortex. Another way in active control is changing vortex core size or strength using jet-blowing from the tip or attaching Canard wing at the blade tip.[22,23]

1.3 Lateral jet blowing method

As one of active control method to reduce the BVI noise, method of jet-blowing from a blade-tip, as shown in Figure 1.4, has been tried by many researchers. The idea of mass injection to control the tip vortex started in the area of fixed wing.

Lee et al.[24-26] have used a wing tip modified with a long single slot to produce a spanwise jet sheet. The effect of this sheet appears to be modification of the lift distribution similar to that produced by an increase in aspect ratio. Unfortunately, the fundamental nature of the tip vortex for the modified wing does not appear to be appreciably altered. Wu and Vakili[27-30] examined the use of discrete wingtip jets for fixed wing to disperse the wake vortex. They have shown that the concept of discrete jets has the potential to effectively disperse the vorticity present in the coherent wing tip vortices. The mechanism for the change appeared to be the formation of multiple auxiliary vortices that decreased the tip vortex strength and introduced increased instability into the flow field. Gowanlock[31] and etc. and other many researchers conducted experimental studies to show jet blowing from a blade-tip can be effective in reducing the strength and velocity gradients of tip vortices. Mineck[32] conducted comprehensive experimental and analytical studies to assess the potential aerodynamic benefits from spanwise blowing at the tip of a moderate-aspect-swept wing.

For the application to helicopter rotor blade, Tan et al.[33] conducted wind tunnel test to reduce BVI noise by blowing compressed air from blade tip of helicopter rotor. They showed that the vortex intensity is reduced while the vortex location is moved outward which resulted in lower BVI noise level. Yamada[34] conducted parametric study using three-dimensional compressible Euler code to calculate the effect of blowing air from blade tip on the tip vortex of single fixed or rotary blade at the various free stream velocities and blowing conditions, such as injection angle, mass flow rate of jet blowing. Yang et al.[35] conducted comprehensive numerical and experimental investigation of the lateral tip-blowing to reduce BVI noise. The results showed that blowing from the wing-tip can diffuse the tip vortex and displace it outward causing the increased 'wing-span'.

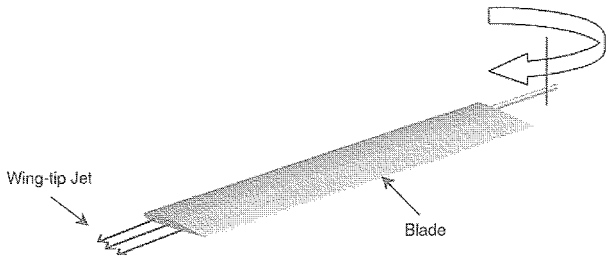

Figure 1.4 Diagram of wing-tip blowing jet of rotor

1.4 Numerical and Experimental Research

The flow field near the rotor must be quantified to fully develop the understanding of the physics of BVI phenomena. Various studies have been carried out by many researchers in the aerodynamic analysis of the helicopter rotor such as the momentum (energy) method by Rankine and Froude, the vortex lattice method and the lifting surface method based on the potential and vortex theory, the methods using the transonic small disturbance equations[36] and advanced full potential equations[37]. However, unlike the Euler and Navier-Stokes equations, these equations cannot take into account the transport of vorticity, the roll-up of the wake following the blade and contraction of tip vortex past the blade, so they are less perfect model for the prediction of aerodynamic loads on rotor blades.

Since the computing power has been increased progressively over the last two decades, the analysis of helicopter rotor flows in hover and forward flight has progressed from the solution of transonic small perturbation equations and full potential equations to that of Euler equations and more recently to that of Navier-Stokes equations. The recent numerical simulation of the flow in the tip region of a transonic swept wing was performed by Mansour[38], and by Kaynak et al.[39] extended to three-dimensional shock-induced separation using a multiblock Euler/Navier-Stokes zonal method. Later Srinivasan[40] have extended the simulation of the flowfield and the vortex-formation around the wing tip region to the transonic flow.

The three-dimensional flow field round a helicopter rotor blade can be characterized mainly in a tip vortex generated at the tip of a rotor blade and a rotating effect by the rotation of the rotor. The tip vortex generated in the backward vortex of a fixed wing of a helicopter rotor blade has a great importance with an aerodynamical view. Since this tip vortex generally occurs in a complex three-dimensional separating flow which is difficult to analyze, most theoretical or experimental researchers have been trying to understand qualitatively the structure of a vorticity transport from a boundary layer near the wing surface to trailing concentrated vortex. The tip vortex is known to cause not only flow instability such as a sudden decrease of an induced drag or a stall in boundary layer but also acoustic noise. Especially in the rotating blades such as propellers or helicopter rotors, more complex vortical wake is occurred by the interaction of following blade than the fixed wing.

1.5 Motivations and Objectives

The preliminary researches, coupled with blowing optimization capabilities[41,42], clearly show the potential benefits of discrete jet blowing as means of active control of wingtip vortex flow to reduce BVI noise. For the control of BVI phenomena or BVI noise, it is necessary to get an exact solution of near filed flow of rotor and far field flow. Main objective of this research work is to study on lateral tip-jet blowing as one of method to reduce BVI noise using compressible flow solver using numerical calculation methods.

In the first part, three-dimensional compressible Euler/Navier-Stokes solver are solved to calculate the effect of flow air from blade tip on the tip vortex of fixed single blade. The computed circumferential velocity profiles of tip vortex are compared with experimental results with single fixed wing as a validation of numerical solver. Then, various flow and jet conditions are applied to the single blade with Freestream Mach numbers 0.5 and 0.8 at the angles of attack of 5 degree. The numerical results include the position of the vortex center along the vortical flow, the size and strength of the rolled tip vortex, and circulation and maximum tangential velocity of the tip vortex. Jet flow from the wing tip can diffuse the tip vortex in the way to make larger core sizes and less velocity gradients, which can be effective way to reduce BVI noise of the rotary wing. The present paper is corresponding to the first part of the research work: the effect of blowing air from blade tip on the tip vortex of fixed single blade.

In the next paper, the predictions of blade vortex interaction noise will be performed using a combined method of an unsteady Euler code with an aeroacoustic code based on Ffowcs-Williams and Hawkings formulation.

Numerical Wind tunnel (NWT) of NAL in Japan will be used to get an accurate aerodynamic flow solution near the rotor blade. The NWT is a parallel super computer which consists if 166 processing elements (PEs). The performance of an individual PE is 1.7 GFLOPS, and each PE had a main memory of 256MB. High-speed cross-bar network connect 166 PEs to make the total peak performance to be about 280 GFLOPS and the total capacity of main memory as much as 45GB. For the calculation of this paper, the typical dividing number along the azimuthal direction is about 2000/rev. The NWT makes it possible to conduct parametric study of the effect of the lateral jet flow on the intensity of the BVI noise.

This research is conducted as a collaborative research program between National Aerospace Laboratory (NAL) in Japan and Pohang University of Science and Technology (POSTECH) in Korea.

2. NUMERICAL METHODS

2.1 Compressible Euler solver

The general governing forms of three-dimensional compressible Euler equations can be written in generalized coordinate system as the followings.

$$\frac{\partial Q}{\partial t}+\frac{\partial F_i}{\partial \xi_i}+H=0$$

where

$$Q = J^{-1}\begin{Bmatrix}\rho\\ \rho u_1\\ \rho u_2\\ \rho u_3\\ e\end{Bmatrix},\quad F_i = J^{-1}\begin{Bmatrix}\rho U_i\\ \rho u_1 U_i + \xi_{i,1}p\\ \rho u_2 U_i + \xi_{i,2}p\\ \rho u_3 U_i + \xi_{i,3}p\\ (e+p)U_i - \xi_{i,t}p\end{Bmatrix},$$

$$H = J^{-1}\begin{Bmatrix}0\\ -\rho\Omega u_2\\ \rho\Omega u_1\\ 0\\ 0\end{Bmatrix}$$

In these equations,

$$(\ )_{,t} = \partial/\partial t, \qquad (\ )_{,j} = \partial/\partial x_j,$$
$$(x_1,x_2,x_3) = (x,y,z), \qquad (\xi_1,\xi_2,\xi_3) = (\xi,\eta,\zeta),$$
$$(u_1,u_2,u_3) = (u,v,w), \qquad (U_1,U_2,U_3) = (U,V,W).$$

And the Jacobian of the transformation is

$$J = \frac{\partial(\xi,\eta,\zeta)}{\partial(x,y,z)} = \left[x_\xi(y_\eta z_\zeta - y_\zeta z_\eta) - x_\eta(y_\xi z_\zeta - y_\zeta z_\xi) + x_\zeta(y_\xi z_\eta - y_\eta z_\xi)\right]^{-1}$$

In the above equations, ρ is the gas density, u, v, w, the Cartesian velocity components in x, y,z directions, and U, V, W are components of contravariant velocity. The quantity Ω is the angular velocity of the blade rotation, and e is the total energy per unit volume. The pressure p is obtained by the perfect gas equation by

$$p = (\gamma - 1)\left[e - \frac{1}{2}\rho(u^2 + v^2 + w^2)\right]$$

where γ is the ratio of specific heats, usually as γ =1.4 for air.

The inviscid flux vectors are discretized using Roe's flux difference splitting (FDS) method[43]. The flux difference across a cell interface is divided into components associated with each characteristic wave with third order accuracy using TVD scheme.[44] TVD scheme has a good capability of capturing the shock wave without adding artificial dissipation. Roe's approximate Riemann solver does not satisfy the entropy condition and thus permits physically inadmissible expansion shock. To remedy this problem, entropy correction is applied [45].

For time integration, Euler Backward Implicit Time Integration is used in the conventional delta form. In order to obtain the unsteady solution in the forward flight condition of helicopter rotor, the Newton iterative method is applied. In this method, the above-mentioned scheme

$$LHS\ \left(Q^{n+1} - Q^n\right) = -\Delta t RHS$$

is modified as

$$LHS\ ^m\left(Q^{m+1} - Q^m\right) = -\Delta t\left(\frac{Q^m - Q^n}{\Delta t} + RHS\ ^m\right)$$

where m means the number of the Newton iteration, In the beginning of the calculation, the steady calculation is conducted at the azimuth angle, $\psi = 90^\circ$ by using the implicit time-marching method. Then, the unsteady calculation is started from this initial condition by using the Newton iterative method. Four iterations are sufficient to reduce the residual at each time-step. The typical dividing number along the azimuth direction is about 1000 per revolution.

2.2 Compressible Navier-Stokes solver

The general governing forms of three-dimensional compressible Navier-Stokes equations can be written in generalized coordinate system as the followings.

$$\frac{\partial Q}{\partial t} + \frac{\partial F_i}{\partial \xi_i} + H = \mathrm{Re}^{-1}\frac{\partial S_i}{\partial \xi_i}$$

where

$$Q = J^{-1}\begin{Bmatrix}\rho\\ \rho u_1\\ \rho u_2\\ \rho u_3\\ e\end{Bmatrix},\quad F_i = J^{-1}\begin{Bmatrix}\rho U_i\\ \rho u_1 U_i + \xi_{i,1}p\\ \rho u_2 U_i + \xi_{i,2}p\\ \rho u_3 U_i + \xi_{i,3}p\\ (e+p)U_i - \xi_{i,t}p\end{Bmatrix},$$

$$H = J^{-1}\begin{Bmatrix}0\\ -\rho\Omega u_2\\ \rho\Omega u_1\\ 0\\ 0\end{Bmatrix},\quad S_i = J^{-1}\begin{Bmatrix}0\\ \xi_{i,j}\tau_{1j}\\ \xi_{i,j}\tau_{2j}\\ \xi_{i,j}\tau_{3j}\\ \tau_{kj}u_k + q_i\end{Bmatrix}$$

The metric notations and the Jacobian of the transformation are same with those of Euler solver.

The variables τ_{ij} and q_i are the stress tensor and heat flux respectively. The hypothesis of eddy-viscosity gives

$$\tau_{ij} = (\mu + \mu_t)\left(u_{i,j} + u_{j,i} - \frac{2}{3}\delta_{ij}u_{k,k}\right),$$
$$q_i = \left(\frac{\mu}{\mathrm{Pr}} + \frac{\mu_t}{\mathrm{Pr}_t}\right)\frac{s_{,i}^2}{\gamma - 1}$$

where μ and μ_t are the molecular and turbulent eddy viscosity, and Pr and Pr_t are the laminar and

turbulent Prandtl numbers which are assumed to be constant values of 0.72 and 0.9 respectively. The quantity s is the speed of sound.

The turbulent eddy viscosity above is calculated with the q-ω turbulent model, which is two-equation model developed by Coakley[46]. Although zero equation models have high numerical compatibility and are effective in attached or weakly separated flows, the algebraic length-scale is difficult to estimate for complex separated flow. And the assumption of equilibrium turbulence makes it impossible to account for flow history or stress-relaxation effect. As solving the partial differential equations directly for both velocity field and length scale of the flow, two-equation models gives good solution for not only isotropic turbulence but also anisotropic complex flows including separation.

In this calculation, the q-ω turbulent model is used due to its numerical compatibility and ability to predict the practical transitional phenomena. The turbulent kinetic energy k and dissipation rate ε are solved by solving the following equations of the field variable q and ω, which have relations of

$q=\sqrt{k}$ and $\omega=\varepsilon/k$.

$$\frac{\partial Q_t}{\partial t}+\frac{\partial F_{ti}}{\partial \xi_i}=\mathrm{Re}^{-1}\frac{\partial S_{ti}}{\partial \xi_i}+H_t$$

where

$$Q_t=J^{-1}\begin{bmatrix}\rho q\\ \rho\omega\end{bmatrix},\quad F_{ti}=J^{-1}\begin{bmatrix}\rho q U_i\\ \rho\omega U_i\end{bmatrix},\quad S_{ti}=J^{-1}\begin{bmatrix}\left(\mu+\dfrac{\mu_t}{\sigma_q}\right)g_{ij}\dfrac{\partial q}{\partial \xi_i}\\ \left(\mu+\dfrac{\mu_t}{\sigma_\omega}\right)g_{ij}\dfrac{\partial \omega}{\partial \xi_i}\end{bmatrix},$$

$$H_t=J^{-1}\begin{bmatrix}\dfrac{1}{2}\left(C_\mu f_\mu\dfrac{s}{\omega^2}-\dfrac{2D}{3\omega}-1\right)\rho\omega q\\ \left[C_1\left(C_\mu\dfrac{s}{\omega^2}-\dfrac{2D}{3\omega}\right)-C_2\right]\rho\omega^2\end{bmatrix}$$

and

$$\mu_t=C_\mu f_\mu\,\mathrm{Re}\frac{\rho q^2}{\omega},\quad f_\mu=1-\exp(-\alpha R),\quad R=\frac{\mu q s}{\rho}\mathrm{Re}.$$

Here, s means normal distance from the wall and $g_{ij}=\nabla\xi_i\cdot\nabla\xi_j$, and the velocity field D and the strain rate invariant S are represented as

$$D=u_{k,k},\quad S=\left(u_{i,j}+u_{j,i}\right)u_{i,j}-\frac{2}{3}D^2$$

Turbulent constants are set to

$$C_1=0.405f_\mu+0.045,\quad C_2=0.92,\quad C_\mu=0.09,$$
$$\alpha=0.0065,\quad \sigma_q=1.0,\quad \sigma_\omega=1.3\ [47]$$

2.3 Grid system and boundary conditions for single blade

Generalized body-fitted curvilinear grid systems can be constructed using C-H-type mesh or H-C-type mesh according to the solver. For the convenience of grid attraction to jet slit area, H-C-type grid may be a proper topology, as shown in Figure 2.1. This grid system is good for concentrating grid near the jet slit of the wing tip, for the slit has comparatively small area with high gradient of velocity. But near the tip region of leading and trailing edge, excessively small grid spacing may cause the calculation unstable. Another typical grid type for wing problem is C-H-type grid system as shown in Figure 2.2. Outer region from the wing tip is set to be branch-cut boundary condition. It is good for well-distributed grid near leading edge of airfoil and easy to create from two-dimensional sectional grid plan, but difficult to put enough grids on jet slit area compared to H-C-type grid.

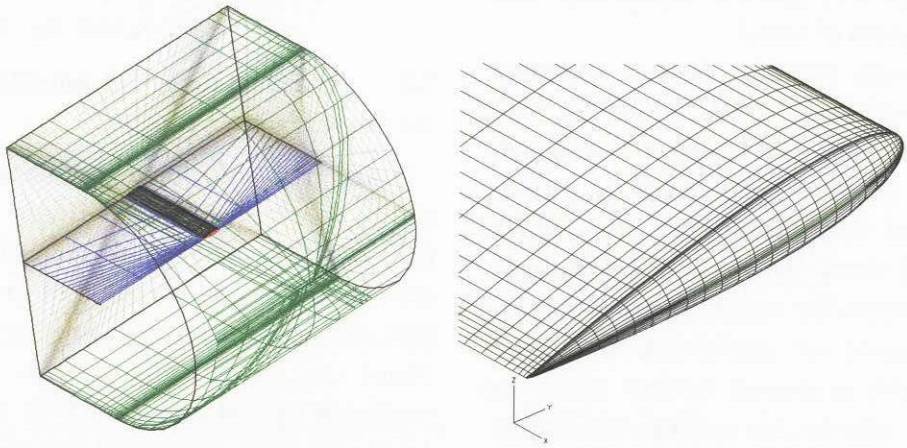

(a) Perspective view *(b) wing-tip and slit*

Figure 2.1 H-C-type grid system

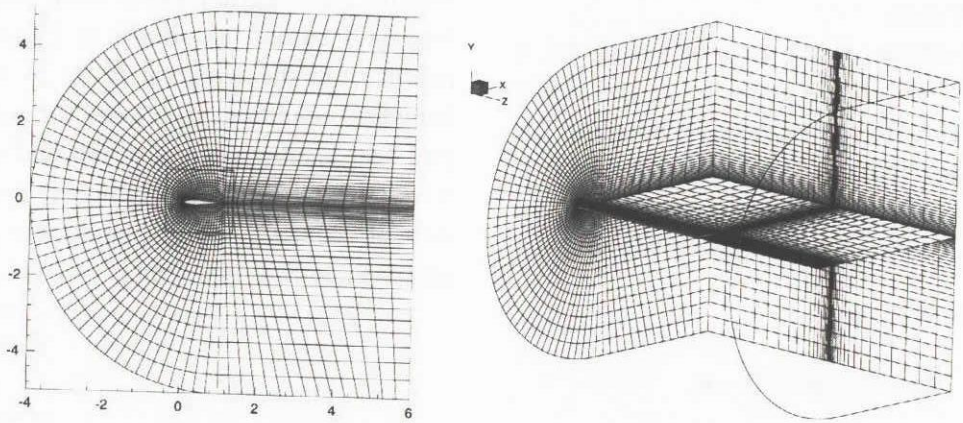

(a) 2-D grid in C-type of NACA0012 *(b) Perspective View*

Figure 2.2 C-H-type grid system

At the surface of the wing, the normal direction component of the velocities are specified to be zero for inviscid Euler computations, which is known as the "no-penetration" condition and can be represented by

$$(v_n)_{wall} = 0$$

At the far-field boundaries, Riemann invariant condition is used as non-reflecting boundary condition, which prevented the outflow effects from entering into the computational region. At the inboard boundary, the flux is set to be zero to permit a cross flow unlike 2-dimensional analysis. This boundary condition is known to have little effect on flowfields. In the region containing the blade root, two kinds of boundary conditions, (a) normal and (b) symmetric boundary condition, is imposed. Even though condition (a) yields better results, this region is not so much dependent on the boundary conditions.

3. RESULTS

3.1 Grid system of a fixed single blade

Comprehensive tip-vortex flow behaviors are numerically analysed in this chapter with a single blade of OLS airfoil section, which had been tested for full-scale aerodynamic experiment and noise data measurement in NASA[48]. Figure 3.1 shows three-dimensional grid systems for single blade

model and detail view of grid system near blade tip. Figure 3.2 shows the sectional grid for blade and tip. The computational domain consisted of C-H-type grid system using 719,656 grid points (chord×normal×span, 181×56×71). The blade tip is simplified to have a sharp edge, where much condensed grids are applied in order to set accurate jet boundary conditions. The jet slit at the tip is located from 20% to 65% of the chord length from the leading edge, and has a slit width of about 20 or 30% of the thickness of the airfoil section. The computational domain has a range of 5-chord lengths in the free-stream region around the blade and a 10-chord length wake region behind the trailing edge. Flow conditions are simplified from one of the flight condition data of helicopter model-rotor experiments. The free-stream Mach number is set to be 0.5 or 0.8, with the angle of attack to be 5 degrees to the free-stream flow. To see the effect of various jet conditions, jet direction, jet Mach number and jet slit area are altered. Considering the outcome of preceding numerical work[49], the variation of jet direction is more specified from –45 degrees forward to 45 degrees backward with an increment of 15 degrees.

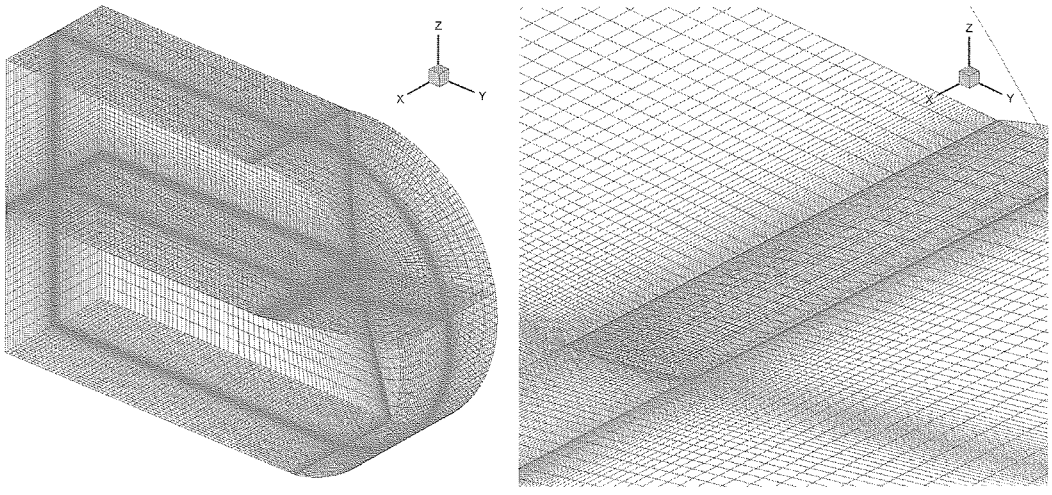

(a) 3D grid system (b) *grid system near blade*

Figure 3.1 Three-dimensional grid systems for single blade model

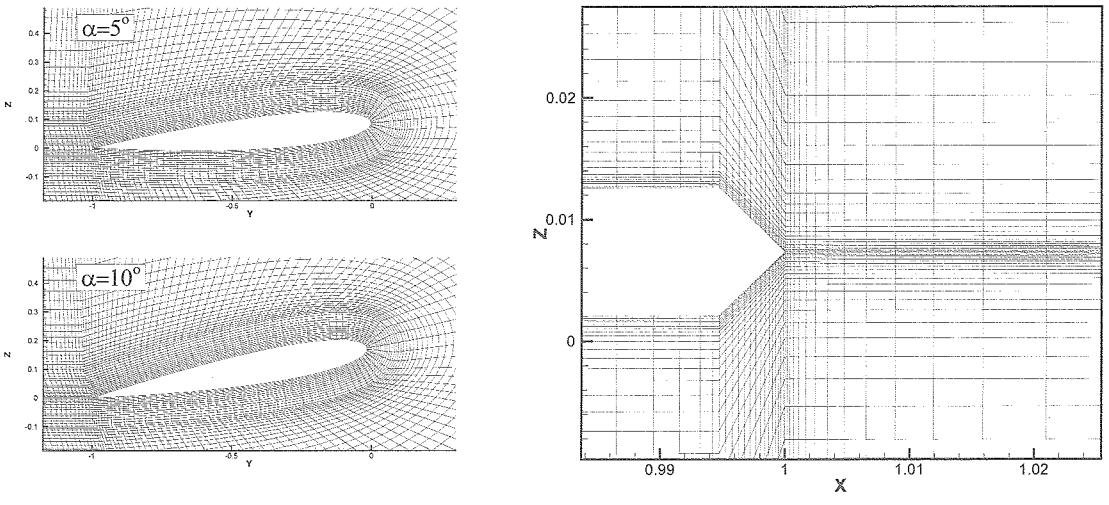

(a) blade geometry *(b) grid distribution near tip*

Figure 3.2 Sectional grid systems for single blade

3.2 Validation of Euler/Navier-Stokes solvers

The computations of tip vortical flow by compressible Euler/Navier-Stokes solvers are performed in order to simulate the vortex behavior induced by the experimental facility of Appendix A. Free-stream Mach number is set to be 0.0882 at the angles of attack of 5 and 10 degrees, which is the same condition as that of experiments. As shown in the diagram of jet flow and tip vortex near tip in Fig. 3.3(a), the circumferential velocity profiles, i.e. the tangential velocity component, of tip vortex of calculation are compared with experimental results as a validation of numerical solver in Fig. 3.3(b),. For convenience of comparison, circumferential velocities and distances from the vortex center are non-dimensionalized by each maximum circumferential velocity and vortex core radius respectively. Although the numerical dissipation appears, the effect of angle of attack on the strength of circulation is reasonably captured by the present code. Furthermore, the profile of circumferential velocity is matched well, implying that this compressible code can be used for the study of tip vortex with jet flow. Figure 3.4 shows the variation of the non-dimensional circulations at 3, 7, 10, 14 chord lengths from trailing edge. The circulations are calculated in the same way of line integral, which is used in experimental results[50], and they are non-dimensionalized by chord length and free-stream velocity. From this figure we can estimate the numerical dissipations along the tip vortex.

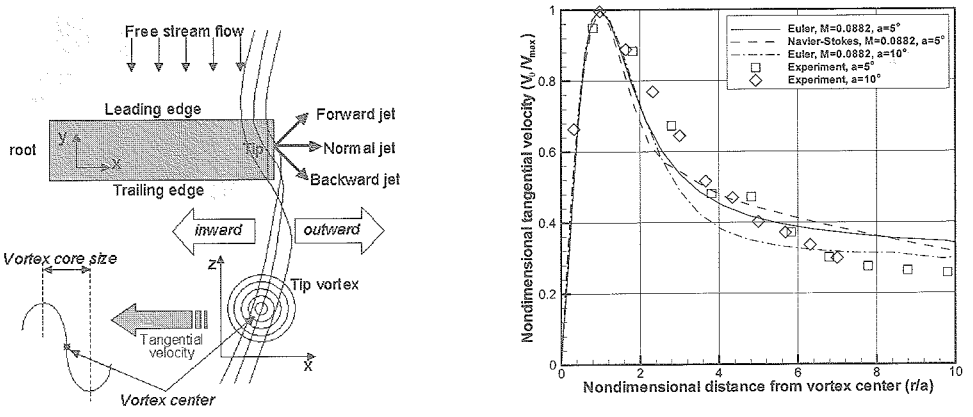

(a) *diagram of jet flow near tip* (b) *Comparison of circumferential velocity profile*

Figure 3.3 Comparison of circumferential velocity profile of tip vortex between experimental and numerical results (square tip, $\alpha = 5^o, 10^o$)

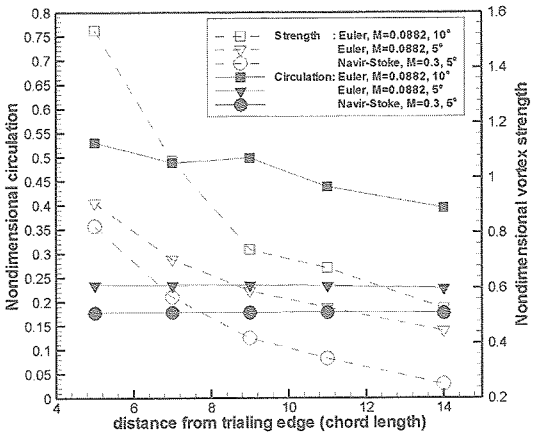

Figure 3.4 Nondimensional circulation at distance from trailing edge for various computations

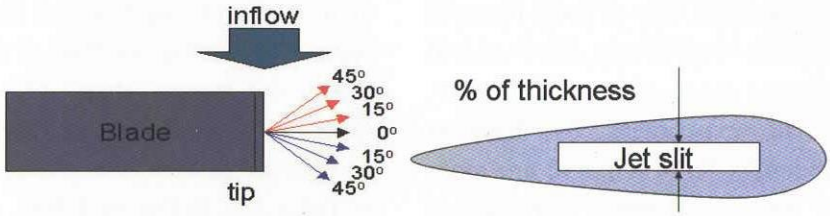

Figure 3.5 Diagram of cases with various tip jet conditions

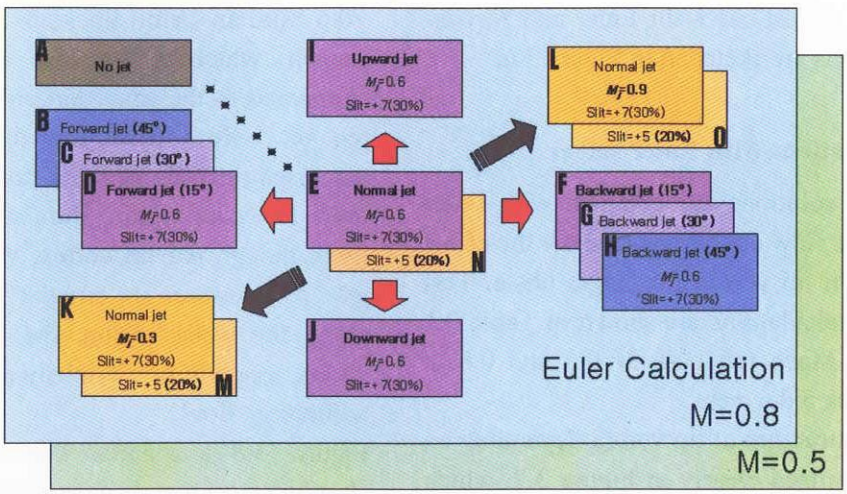

(a) Euler calculation

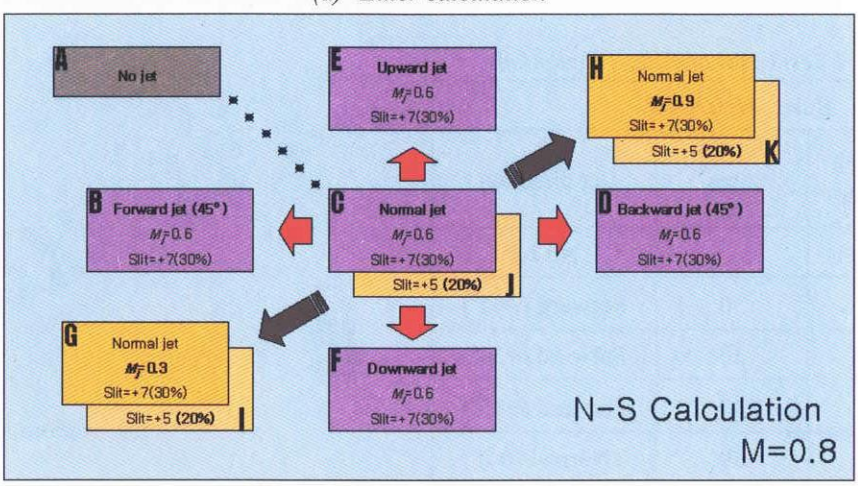

(b) Navier-Stokes calculation

Figure 3.6 Diagram of test cases for Euler and Navier-Stokes calculations

3.3 Various jet flow parameters

Figure 3.5 shows the diagram of cases with various directions of tip jet flow and jet slit area. Forward jet is defined to have jet direction against the free stream flow, while normal jet means the jet flow with the right angle with respect to the free stream flow. Backward jet is blowing the free-stream flow. This calculation is conducted with single grid of single fixed blade as the preliminary study. The same condition will be calculated with overlapped fine grid system for forward flight condition. The shape of jet slit is rectangular, and two different cases for jet slit area are calculated.

Various jet condition are simulated to study the effect of parameters such as jet Mach number, jet slit area, and jet direction for two freestream Mach numbers, which represent the tip Mach number of

advancing side and retreating side of rotor blade in moderate flight condition respectively. Forward and backward jet conditions are considered important from the results of experiment by Kawada Industries, Inc. (Appendix A.3[57,58]), and are more specified using 15 degrees increase. For Navier-Stokes solution, smaller numbers of cases are solved because of computing ability and time. The whole diagrams of test cases for Euler and Navier-Stokes calculations are sketched in Figure 3.6.

3.4 Calculations with Euler solver

Inviscid flow solutions are obtained with Euler solver for various flow conditions to show the effect of tip jet flow on tip vortex for single blade. Test cases for Euler calculations are shown in Table 3.1 with freestream Mach numbers M=0.5 and 0.8 at the angle of attack 5 degrees.

The different structure of tip vortex depending on jet flow are visualized clearly in Figure 3.7, which shows traces of tip vortex by the vorticity contours up to 10-chord length behind the trailing edge of the blade with/without jet flow at M=0.8. Figure 3.7(a) shows the typical shape of wake spiral and its formation to be the tip vortex from the fixed wing without jet flow, which is corresponding to case ***A*** at Table 3.1. In Figure 3.7(b), air is injected at the tip in a normal direction to the free-stream in a spanwise direction with a jet Mach number of M_j =0.6 from an airfoil thickness of the 30% width of jet slit, which is the case ***E*** at the Table 3.1. Compared to the small but clear tip vortex without jet, jet flow from the tip makes tip vortex dispersed not only near the tip region but also up to quite far-wake region, showing bigger vortex size. Even though the tip vortex, which is disturbed by jet flow, restores its circular shape as it proceeds along the wake region, the core size of the tip vortex seems to be obviously different from the one without jet flow.

Figure 3.8 compares velocity vectors at the chordwise sectional plane (70% chord-length from leading edge) of the blade and vorticity contours at

Table 3.1 Test cases of Euler calculations

Euler, M=0.5, 0.8			
Case	Jet Mach number	Jet slit Area (%)	Jet direction
A	-	-	No Jet
B	0.6	30	Forward (+45°)
C	0.6	30	Forward (+30°)
D	0.6	30	Forward (+15°)
E	0.6	30	Normal (0°)
F	0.6	30	Backward (-15°)
G	0.6	30	Backward (-30°)
H	0.6	30	Backward (-45°)
I	0.6	30	Upward (+45°)
J	0.6	30	Downward (-45°)
K	0.3	30	Normal (0°)
L	0.9	30	Normal (0°)
M	0.9	20	Normal (0°)
N	0.6	20	Normal (0°)
O	0.9	20	Normal (0°)

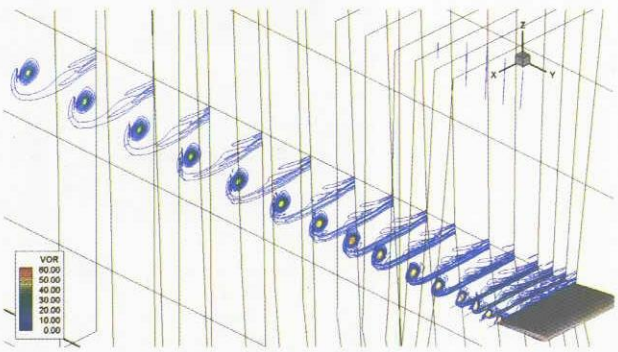

(a) *without jet flow*

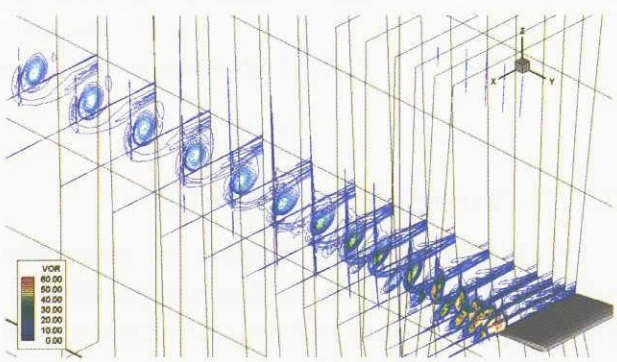

(b) with normal jet flow

Figure 3.7 Comparison of vorticity contours upto L=10C distance for with/without jet flow (Euler, $\alpha = 5^o$, M=0.8, M_j=0.6)

the 10 chord length behind trailing edge. Vector plots shows effect of jet flow on the formation of the attached vortical flow, which would be developed into tip vortex as it leave the trailing edge. Compared to the small vortex of the case without jet, jet flow accelerates the induced flow to make the vortical motion larger. This enlarged vortical motion consequently causes the bigger vortex size, as shown in the vorticity contour.

Figure 3.9 shows crossflow velocity vectors and formation of tip vortex at the mid-section of 90% chord length at 5-degree angle of attack with freestream Mach number M=0.8. Compared to the typical rollup process originating the tip vortex close to tip region as seen in Figure 3.9(a), the jet flow produces more complicated structure of tip vortex in Figure 3.9(b). As jet flow begins near the leading edge in the normal direction, it plays a role in extending the wing-span, and the rollup flow, which is driven by the pressure difference between the upper and lower surfaces, and also follows the extended span away from the tip. As a consequence of this outward-driven rollup flow due to the jet flow, the induced spiral flow, vortex ***a***, is located at a distance from the tip. As long as the jet flow is maintained blowing, vortex ***a*** continues to elongate outward and upward, which could get separated into two vortices, vortex ***a*** and vortex ***b***. When the jet is no longer blowing near the trailing edge on tip, the rollup flow tries to come over onto the upper surface directly to generate a small secondary swirling flow, vortex ***c***, attached on the tip near the upper surface. Departed from the trailing edge into a wake region, vortex ***c*** is observed to disappear, and vortex ***a*** and ***b*** grows to merge together as a well-organized spiral character of tip vortex, being a larger core size, which is considered as one of main contributions of jet flow.

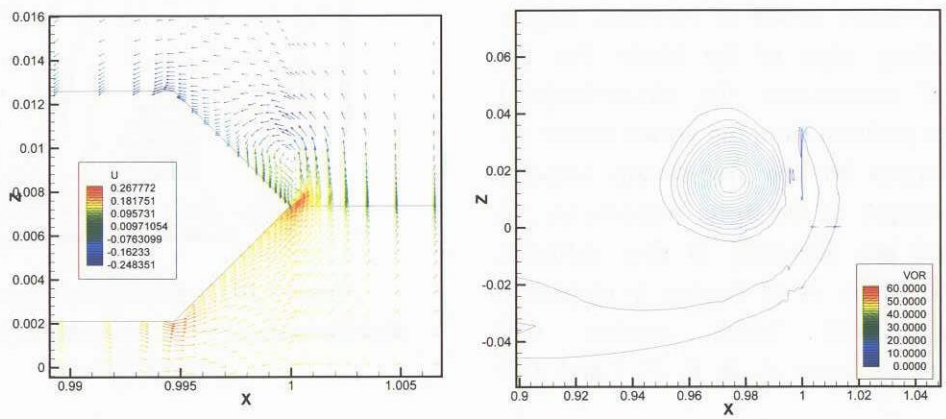

(a) No jet

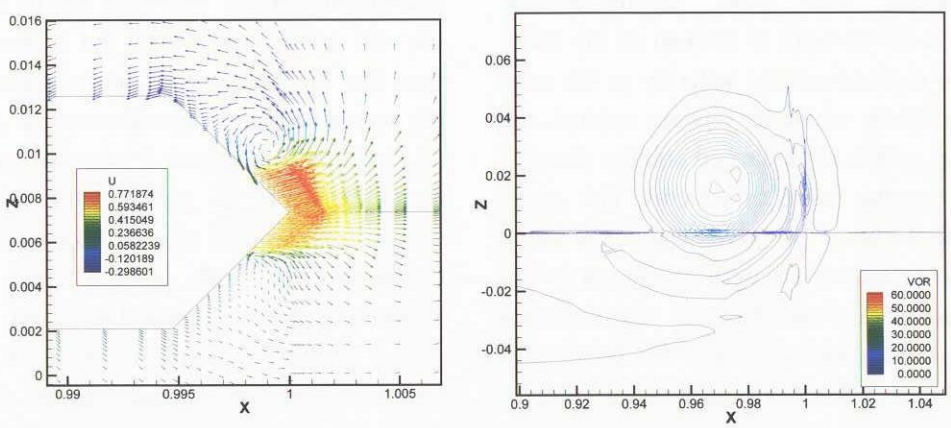

(b) Normal Jet

Figure 3.8 Comparison of velocity vectors and contours various jet, directions (Euler M=0.8, M_j=0.6)

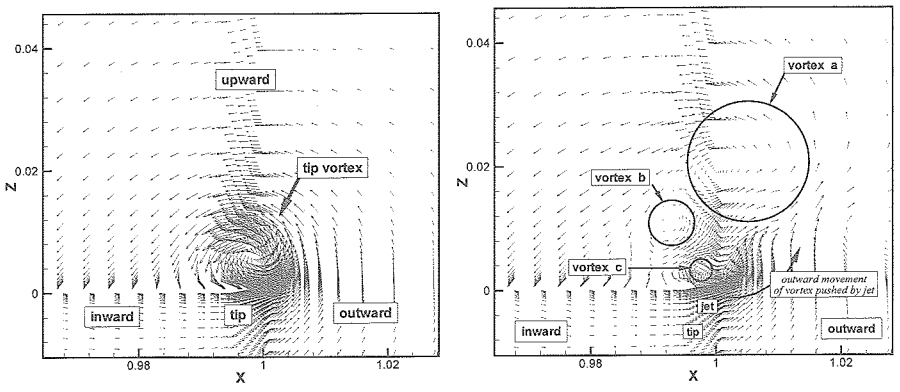

(a) nojet *(b)normal jet (M_j=0.6)*

Figure 3.9 Crossflow velocity vectors at mid-section of 90% chord length for tip vortex formation (Euler, $\alpha = 5^o$, M=0.8)

The effects of various jet flows on the core size and the strength of tip vortex can be compared more clearly with velocity profiles at the vortex center. Figure 3.10 shows the characteristic circumferential velocity distributions for various jet directions with respect to each vortex center at 10-chord lengths behind the trailing edge of the blade. For the convenience of comparison, the circumferential velocity and the position from the vortex center are non-dimensionalized by the free-stream velocity and the chord length of the blade respectively. In this figure, jets are dispersed in four different directions at the angles of 45 degrees in respect to the x-direction with Mach number 0.6, corresponding to the cases ***A***, ***B***, ***E***, ***F***, ***I*** and ***J*** in Table 3.1.

The core size of the tip vortex is defined as the distance between two peak circumferential velocities, while its strength is defined as the mean gradient of the circumferential velocity to the core size. From the figure, whatever jets are applied, the core sizes of tip vortex are enlarged and the strength of tip vortex became weak in general. The graph shows that the forward jet gives most favorable effect on the core size or strength of the vortex. In the case of backward flow, the core size becomes larger, and thus the vortex strength can be smaller even though the maximum circumferential velocity becomes slightly larger.

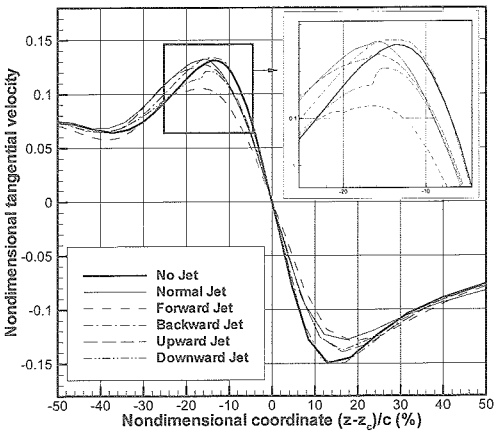

Figure 3.10 Comparison of tangential velocity distributions at L=10C according to jet directions (M=0.8, M_j=0.6)

Figure 3.11 efficiently illustrates the correlation between the vortex core size and its strength for all the test conditions. From the figure, it is clearly seen that the smaller the core size gets, the stronger the vortex becomes regardless of the jet flow. When jet direction alters from forward to backward (cases ***B***, ***C***, ***D***, ***E***, ***F***, ***G***, and ***H***), the overall tendency shows that the core size decreases and its strength increases for both M=0.8 and M=0.5 with exceptions of some forward jet flows.

The case of forward jet at 15 degree (case ***D***) shows similar phenomena with the case of normal jet (case ***E***), but the forward velocity component appears to disturb the opposite free-stream to dominate the jet flow in normal direction, which results in stronger outward movement of rolled-up vortex than that of the normal jet case. Therefore

forward jet is more effective in improving the jet effect of larger core size. Increasing injection angle (case *C* of *M*=0.8) can amplify the jet effect, but when forward velocity component becomes too large with respect to free-stream flow (case *B* of *M*=0.8), excessive disturbance on flow may bring about a counter effect, as observed in the correlation figures. In the flow of smaller free-stream Mach number (*M*=0.5), the forward jet has relatively stronger effect in producing instability easily than the larger free-stream Mach number (*M*=0.8). As a consequence of the counter effect, the cases of higher dispersion angle (cases *B* and *C* of *M*=0.5) show the core size of vortex smaller and its strength stronger than those with lower injection angle (case *D* of *M*=0.5).

Even though the case of backward jet at 15 degrees (case *F*) also shows a similar phenomenon with the case of normal jet (case *E*), the backward velocity component causes not only rollup flow acceleration to make a strong vortex, but also secondary vortex delay, which causes earlier inward-movement of existing vortex to make a smaller vortex core size. Therefore even the normal velocity component of 15-degree backward jet comes up to almost 96.6% of that of normal jet, the core size of vortex gets smaller and its strength grows stronger with backward jet conditions. As the injection angle increases, the phenomena of backward jet approach that of no jet case.

When the jet changes from upward to downward (cases *I*, *E*, and *J*), there is no clear pattern in the change of core size and strength. Upward and downward jet flows show a similar mechanism of vortex formation, but the positions of rollup vortex and secondary vortex are different depending on the jet direction. Upward jet flow produces vertically-biased rollup vortex, and the secondary vortex originates close to the tip under the existing vortex. Downward jet flow prevents the rollup flow from coming up to the upper surface in the similar way as a stronger jet extending wing-span. This extended span produces horizontally-biased rollup vortex, and the secondary vortex is located inward on the left of the existing vortex. Even though downward dispersion seems more effective in the way of larger core size for some cases, the complex structure of vortex merging makes it difficult to generalize the effect of upward jet and downward jet.

Considering the variations of jet Mach number (cases *K-E-L* or *M-N-O*) and slit area (cases *M-K*, *N-E* or *O-L*), each larger jet area and higher jet Mach number produces bigger disturbance into the tip vortex to make core size larger and vortex strength less. Even though there are many variations in core size and strength according to the jet conditions, it is certain that core sizes of tip vortex are enlarged and their strength becomes weaker under any kind of jet condition compared to that without jet (case *A*).

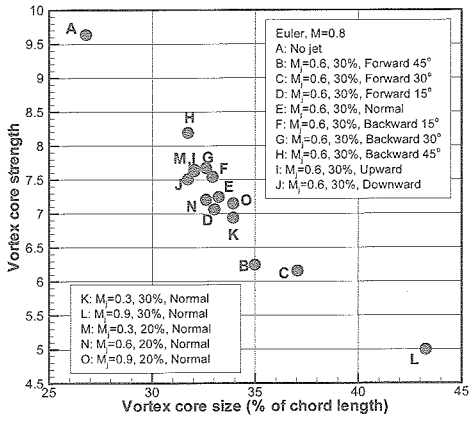

(a) M=0.8

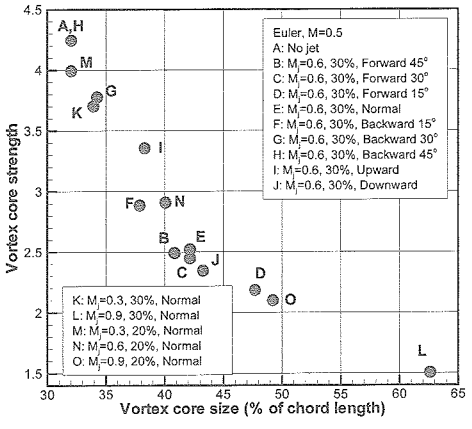

(b) M=0.5

Figure 3.11 Comparison of vortex core size and strength with various jet directions(Euler, M=0.8, 0.5)

As mentioned before, the core size of tip vortex and its strength are important parameters on BVI noise generation, which is in direct proportion to the magnitude of pressure gradient on the blade surface. The pressure on the surface undergoes a rapid

change when a blade bumps against the tip vortex generated from the preceding blade. The bigger the core size becomes, the less the pressure gradient would be, implying that the smaller BVI noise would be developed. In the same way, the weaker strength of the tip vortex would make BVI noise smaller. Therefore the results with fixed blade show that jet flow can play a positive role in reducing BVI noise by increasing the core size and decreasing the strength of tip vortex.

Figure 3.12 shows the positions of the vortex center at 10-chord length behind the trailing edge of the blade for various jet conditions. Even though the jet flow tends to displace the tip vortex outward causing an increase of wing span near tip region, the vortex center is dragged inward as tip vortex developed compared to the tip vortex without jet.

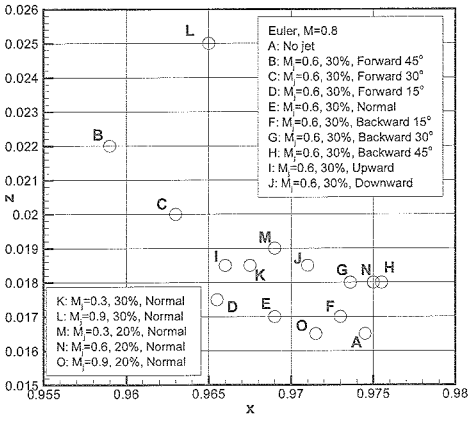

(a) M=0.8

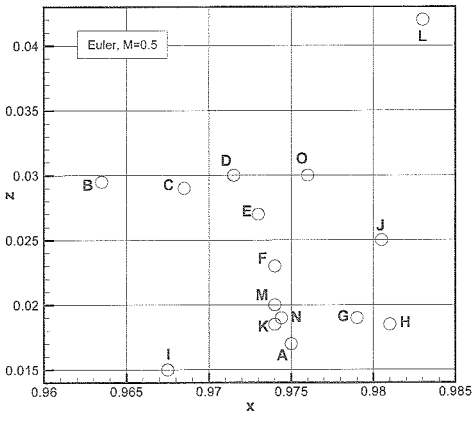

(b) M=0.5

Figure 3.12 Comparison of vortex position in x- and z-axis with various jet directions(Euler, M=0.8, 0.5)

The positions of the tip vortex with forward jet indicate that as jet injection angle decreases (cases *B*, *C*, *D*, *E*, and *F*), the vortex center moves outward to approach the position of vortex without jet (case *A*). But when backward injection is too strong (cases *G* and *H*), the positions of the tip vortex exceed outward that of vortex without jet. The same pattern can be seen when the direction of jet is changed from upward to downward (cases *I*, *E* and *J*). Even though the change of vortex positions are lack of consistency depending on jet slit area and jet Mach number, every jet condition push the center of vortex upward compared to the one without jet (case *A*). Since severe BVI noise is considered to occur when parallel interaction happens during descent flight, upward movement of tip vortex may increase miss-distance between blade and vortex resulting in the reduction of BVI noise. So, the above figure implies that jet flow can also play a positive role in reducing BVI noise in a way of increasing miss-distance.

3.5 Calculations of single blade with Navier-Stokes solver

The viscous effect is examined with the solution using Navier-Stokes solver for the same free-stream flow and jet conditions as used in Euler calculations with a Reynolds number of 1.77×10^7 based on the chord length. The free-stream flow and jet conditions are listed in Table 3.2.

Table 3.2 Test cases of Navier-Stokes calculations for free stream Mach number, jet Mach number, slit area, and jet direction

Navier-Stokes, M= 0.8			
Case	Jet Mach number	Jet slit Area (%)	Jet direction
A	-	-	No Jet
B	0.6	30	Forward (+45°)
C	0.6	30	Normal (0°)
D	0.6	30	Backward (-45°)
E	0.6	30	Upward (+45°)
F	0.6	30	Downward (-45°)
G	0.3	30	Normal (0°)
H	0.9	30	Normal (0°)
I	0.3	20	Normal (0°)
J	0.6	20	Normal (0°)
K	0.9	20	Normal (0°)

The viscosity of Navier-Stokes calculations produces much dissipation to make larger core size and thus weaker vortex strength. Figure 3.13 shows the comparison of tip vortices resulted from Euler and Navier-Stokes calculations by comparing the vorticity contours and circumferential velocity profiles of vortex cores at 10-chord length behind the trailing edge. As mentioned above, viscous computations show larger vortex core sizes in vorticity contours and much less gradient in the velocity profiles, which in turn means less vortex strength compared to the those from inviscid computations. And the effects of jet flow on tip vortex show same tendencies just as in Euler computation, i.e. larger core size and smaller strength.

Figure 3.14 shows the distribution of vortex core size and vortex strength for various jet conditions. The overall variation shows the similar pattern with that of Euler computations. The core size of tip vortex is enlarged and its strength became smaller compared to those without jet (case *A*) once jet flow is applied at any condition. Figure 3.15 shows the positions of the vortex center at 10 chord lengths behind the trailing edge of the blade at various jet

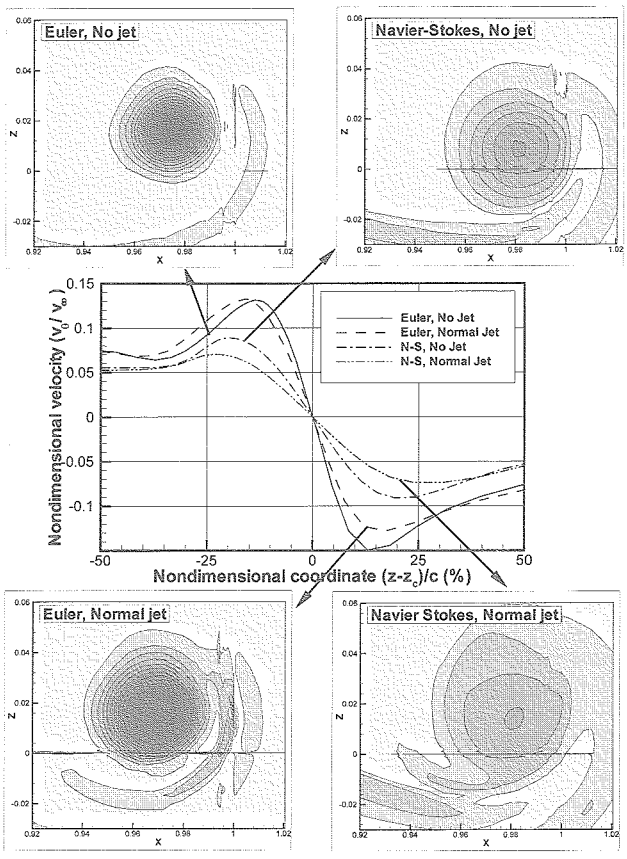

Figure 3.13 Comparison of tip vortex between results of Euler and Navier-Stokes calculations (M=0.8, M_j=0.6)

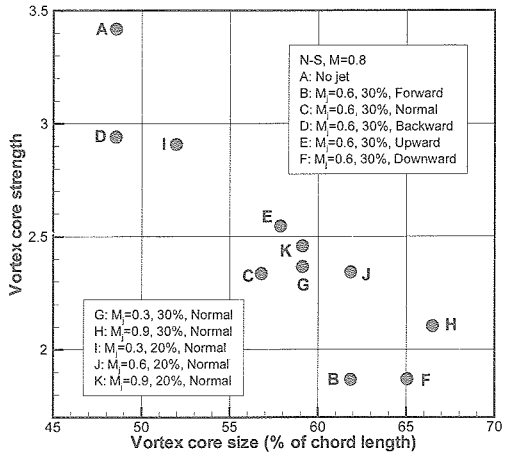

Figure 3.14 Comparison of vortex core size and strength with various jet directions(Navier-Stokes, M=0.8)

conditions, which shows the same effects to push the center of vortex spanwise outward. Viscosity affected the repositioning of tip vortex, but the behavior of movement remains similar to inviscid results.

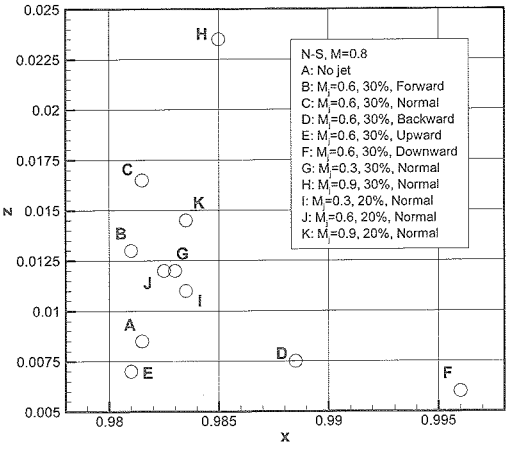

Figure 3.15 Comparison of vortex position in x- and z-axis with various jet directions (Navier-Stokes, M=0.8)

4. SUMMARY AND CONCLUSIONS

As one of the active control method to reduce Blade-Vortex Interaction (BVI) noise of helicopter rotor, the effects of lateral wing-tip jet flow are analyzed for the generation and behavior of tip vortical flow from fixed single blade. Comprehensive numerical investigations on the tip vortical characteristics with Euler/Navier-Stokes solvers are performed for various conditions to get the following conclusions.

(1) Numerical results show that the compressible solvers are valid for further study on the flow phenomena with jet flow. Jet flow has effects on tip vortex to weaken the vortex strength and enlarge its core size compared to those without blowing. Also jet flow moves tip vortex upward and outward which increases miss-distance when BVI occurs.

(2) Comparing the results of various jet conditions, moderate forward jet is found to be more effective than normal or backward jet. Although upward/downward blowing doesn't show consistency contribution to the behavior of the tip vortex, downward injection is proved to be more effective in the way of bigger core size. Increasing jet Mach number or slit area makes the tip vortex be of larger core size and weak strength.

(3) In spite of a lot of varieties of structure and behavior of tip vortices depending on jet conditions, any kind of jet could produce larger core size and weak strength of tip vortex than those without jet. As a result, lateral jet blowing can be positively applied to the helicopter rotor for reducing BWI noise.

With these results above, the method to use jet blowing can be effective way to reduce the peak noise in the helicopter BVI phenomena.

REFERENCES

[1] Brook,T.F., Jolly,J.R., Marcolini,M.A., *Helicopter main-rotor noise*, NASA Technical Paper 2825, 1988

[2] Seath, D.D. and D.R. Wilson., *Vortex-airfoil interaction tests*, AIAA 86-0354, 1986

[3] Baeder, J.D., J.M. Gallman, and Y.H. Yu., *A computational study of the aeroacoustics of rotors in hover,* J. of American Helicopter society, Vol.42, No.1 pp.39-53, 1997

[4] Devenport, W.J., C.M. Vogel, and J.S. Zsoldos., *Flow structure produced by the interaction and merger of a pair of co-rotating wing-tip vortices,* J. of Fluid Mech., Vol.394, pp.357-377, 1999

[5] Ham, N.D., *Some conclusions from an investigation of blade-vortex interaction*, J. of American Helicopter society, Vol.20, No.4, pp.26-31, 1975

[6] Matthewson, C.S., Vakili, A.D. and Gowanlock, D.K., *Adaptive control of wingtip vortex flows*, AIAA, 98-0318, 1998

[7] Vakili, A.D., Matthewson, C.S. and Gowanlock, D.K., *Control of helicopter blade tip vortex*, AIAA, 98-2240, 1998

[8] Saito, S., Aoyama, T., Ochi, A., Kondo, N. and Yamaguchi, A., *Impulsive noise calculation using moving overapped grid method/ Kirchhoff method*, 25th European Rotorcraft Forum, B2:1-11, 1999

[9] Hassan, A.A., Straub, F.K. and Charles, B.D., *Effects of surface blowing/suction on the aerodynamics of helicopter rotor blade-vortex interaction (BVI) - A numerical simulation*, J. of American Helicopter society, Vol.42:182-194, 1997

[10] Tung, C., Caradonna, F. X. and Johnson, W., *The prediction of transonic flows on advancing rotors*, Journal of American Helicopter Society, Vol.

31, pp.4-9, 1986

[11] Boniface, J. C. and Pahlke, K., *Calculations of multibladed rotors in forward flight using 3D Euler methods of DLR and ONERA*, 22nd European Rotorcraft Forum, 1996

[12] Boniface, J. C., Mialon, B., and Sides, J., *Numerical simulation of unsteady Euler flows around multibladed rotors in forward flight using a moving grid approach*, AHS 51st Annual Forum, 1995

[13] Ochi, A., Shima, E., Aoyama, T., Saito, S. and Yamakawa, E., *BVI noise prediction by moving overlapped grid method*, AHS 55th Annual Forum, 1999

[14] Tadghighi, H., Hassa, A., and Charles, B., *Prediction of blade-vortex interaction noise using airloads generated by a finite-difference technique*, AHS 46th Annual Forum, 1990

[15] Yu, Y.H., Tung, C. and Gallman, J., *Aerodynamics and acoustics of rotor blade-vortex interaction,* Journal of Aircraft, Vol.32, No.5, pp.970-977, 1995

[16] Caradonna, F. et al., *A review of methods for the prediction of BVI noise*, AHS technical specialist' meeting for rotorcraft acoustics and aerodynamics, 1997

[17] Aoyama, T., Kawachi, K., Saito, S. and Kamio, J. *Unsteady analysis of transonic helicopter rotor noise*, 19th European Rotorcraft Forum, 1993

[18] Aoyama, T., Kondo, N., Aoki, M., Nakamura, H. and Saito, S. *Calculation of rotor blade-vortex interaction noise using parallel super computer*, 22nd European Rotorcraft Forum, 1996

[19] Jacklin, S.A. and Nguyen, K. Q., *Full-scale wind tunnel test of a helicopter individual blade control system,* 50th Annual Forun of the Americal Helicopter Society, 1994

[20] Splettstoesser, W., R. Kube, W. Wagner, et al., *Key results from a higher harmonic control aeroacoustics rotor test (HART),* J. of American Helicopter society Vol.42, No.1 pp.58-78, 1998

[21] Hassan, A. A., Charles, B. D., Tadgahighi, H. and Sankar, L. N., *Blade-mounted trailing edge flap control for BVI noise reduction*, NASA Contractor Report 4426, 1992

[22] Araki, R., Obayashi, S., Nakahashi, K., Tsukahara, T., Obukata, M., and Nakadate, M., *A numerical method for blade vortex using vortex confinement*

[23] Ota, T., Hashiguchi, Y., Tsukahara, T., Obukata, M., and Nakadate, M., *BVI noise reduction with Canard blade tip* (1st Report)

[24] Lee, C.S., Tavella, D., Wood, N.J. and Roberts, L., *Flow structure and scaling laws in lateral tip blowing*, AIAA Journal, Vol.27, No.8, Paper No.86-1810, 1988

[25] Lee, C.S., Tavella, D., Wood, N.J. and Roberts, L., *Lift modulation with lateral wing-tip blowing*, Journal of Aircraft, Vol.25, No.4, 1988

[26] Lee, C.S., Tavella, D., Wood, N.J. and Roberts, L., *Influence of wing-tip configuration on lateral bowing efficiency*, AIAA 24th Aerospace Science Meeting

[27] Wu, J.M., Vakili, A.D. and Chen, Z. L., *Wing tip jets aerodynamic performance*, Proceedings of the 13th Congress of the International Council of the Aeronautical Science, ICAS 82-5.6.3, 1982

[28] Wu, J.M., Vakili, A.D. and Gilliam, F.T., *Aerodynamic interaction of wingtip flow with discrete wingtip jets*, AIAA Paper 84-2206, 1984

[29] Wu, J.M., Vakili, A.D. and Mo, J.D., *Investigation of phenomena of discrete wingtip jets*, UTSI Report 88-06

[30] Wu, J.M., Vakili, A.D. Chen, Z.L., and Gilliam, F.T., *Investigation of the effect of discrete wingtip jets*, AIAA Paper 83-0546, 1983

[31] Gowanlock, D.K. and Matthewson, C.S., *Control of rotor tip vortices*, AIAA, 99-0012, 1999

[32] Mineck, R.E., *Study of Potential Aerodynamic Benefits From Spanwise Blowing at Wingtip*, NASA Technical Paper 3515, 1995

[33] Tan, A., Hara, Y. and Shindo, S. *Reduction of BVI noise by blowing air from blade tip*, Japanese Aircraft Symposium, 35th:73-76; 1997

[34] Yamada, L., *Numerical Analysis of Tip Vortex Generated by Helicopter Blade,* Dissertation of M.S., Science University of Tokyo, 1999

[35] Yang, C.M., Baek, J.H., Saito, S., Shirai, M., Suenaga, H, Yamada, R., Nishizawa, U., Tan, A. Kanehira, N., and Shindo, S., *Numerical and experimental investigations of tip vortex with lateral wing-tip blowing*, 26th European Rotorcraft Forum, 2000

[36] Caradonna, F.X. and Isom, M.P., *Subsonic and*

transonic potential flow over helicopter blades, AIAA Journal, Vol.10, pp.1606-1612, 1972

[37] Strawn, R.C. and Caradonna, F.X., *Numerical modeling of rotor flows with a conservative form of the full-potential equation*, AIAA Paper 86-0079, 1986

[38] Mansour, N. N., *Numerical Simulation of the Tip Vortex Off a Low-Aspect Ratio Wing at Transonic Speed*, AIAA Journal, Vol.23, Aug., pp. 1143 –1149, 1985

[39] Kaynak, U., Holst, T., Cantwell, B. J., and Sorenson, R. L., *Numerical Simulation of Transonic Seperated Flows over Low-Aspect Ratio Wings*, *Journal of Aircraft*, Vol.24, Aug., pp. 531-539, 1987

[40] Srinivasan, G. R., McCroskey, W., J., Baeder, J. D., and Edwards, T. A., *Numerical Simulation of Tip Vortices of Wings in Subsonic and Transonic Flows*, *AIAA Journal*, Vol.26, Oct., pp. 1153-1162, 1988

[41] Wu, J. M., Vakili, A. D. and Gilliam, F. T., *Aerodynamic interaction of wingtip flow with discrete wingtip jets*, AIAA Paper 84-2206, 1984

[42] Wu, J. M., Vakili, A. D. and Mo, J. D., *Investigation of phenomena of discrete wingtip jets*, UTSI Report 88-06, 1988

[43] Roe, P.L., *Approximate Riemann solvers, parameter vectors, and differenece schemes*. Journal of Computational Physics, Vol.43:357-372, 1981

[44] Bram van Leer, *Flux-Vector Splitting For The Euler Equations*, Lecture Notes on Physics, Vol. 170, pp. 507-512, 1982

[45] Katz, J. and Plotkin, A., *Low-Speed Aerodynamics - From Wing Theory to Panel Methods*, McGraw-Hill Inc., pp.331-342

[46] Coakley, T. J., *Turbulence modeling methods for compressible Navier-Stokes equations*, AIAA paper 83-1693, 1983

[47] Aoyama, T., Saito, S. and Kawachi, K., *Navier-Stokes analysis of blade tip shape in hover*, 16th European Rotorcraft Forum, 1990

[48] Boxwell, D.A., Schmitz, F.H., Splettstoesser, W.R. and Schults, K.J., *Helicopter model rotor-blade vortex interaction impulsive noise: scalability and parametric variations*, J. of American Helicopter society Vol.32, No.1 pp.3-12, 1987

[49] Yang, C., Baek, J., Saito, S., Shirai, M., Suenaga, H., Yamada, R., Nishizawa, U., Tan, A., Kanehira, N., and Shindo, S., *Numerical and Experimental Investigations of Tip Vortex with Lateral Wing-Tip Blowing*, 26th European Rotorcraft Forum, 2000

[50] Nishizawa, U., *Experimental study on the behavior of tip vortex*, M.S. Thesis, Tokyo Noukou University, 2001

[51] *Research development to reduce the helicopter rotor noise*, 1996, Report No.0706 in Kawada Industries Inc.

[52] *Research development to reduce the helicopter rotor noise*, 1997, Report No.0803 in Kawada Industries Inc.

APPENDIX A.

Experimental Research for Tip Blowing Method in Kawada Industries, Inc.

The experiments are carried out in Gottingen-type Low-speed wind tunnel of National Aerospace Laboratory (NAL) of Japan, which has 75m length, 25m width. The test section was 5.5m wide, 6.5m high, 9.5m long with octagon-shape, which was made by cutting 1 m at each corner of rectangular test section. It has single-stage axial blower directly connected to a driving motor with 10-bladed variable-pitch rotor of 9.3m diameter and 8-bladed stator installed downstream of the rotor. The capacity of motor is 3,000 kW with 30 - 214 RPM to produce the wind of 1m/s ~ 70m/s speed by changing the dynamic pitch angle and rotational speed.

The experiments are conducted with vortex generator of a 350mm-chord-length NACA0012 airfoil which has 2100mm span length, as shown in Figure A.1. The blade model was made from Aluminium alloy (A7079). The model was attached to Model Support System of the wind tunnel and the angle of attack can be altered from -10 to 10 degrees. Also, the blade tip can be changed with different shapes. Figure A.2 shows two kinds of wing tip shape, rectangular and tapered tip. Rectangular tip has tip-span length, c=350mm, and tip-chord length, b_t=350mm. Tapered tip has tip-span length, c=350mm, and tip-chord length,

b_t=350mm, which decrease to be 1/3 at the tip.

A 7-hole yaw probe measurement system was used to measure the time-average velocity in turbulent flow with calibration procedure. The probe used in this study has a stem of 6.1mm in outer diameter and 4.8mm in inner diameter. Within the stem are seven tubes, each of internal diameter 1.1mm. The tip of the probe is machined in a conical shape with a half-angle 30 degrees. The tip vortex was visualised using Laser Light Sheet (LLS) technique with 4W argon-laser and smoke generator. The equipment system in the test section was shown in Figure A.1, and the vortex/smoke generator was shown in Figure A.3. The objectives of this experiment are to study tip vortex structure (1) to compare with mathematical models and (2) to check the effect of tip shape on tip vortex.

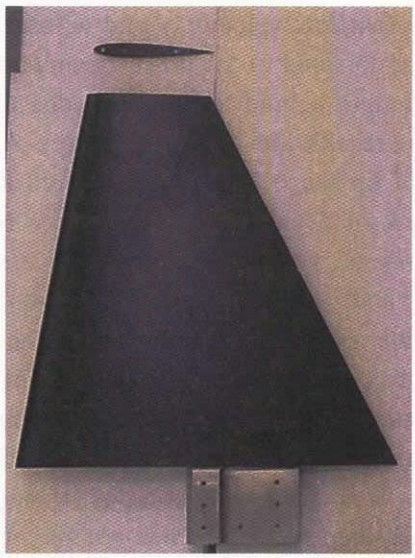

(b) tapered tip

Figure A.2 Two Tip Shape for Wing Model

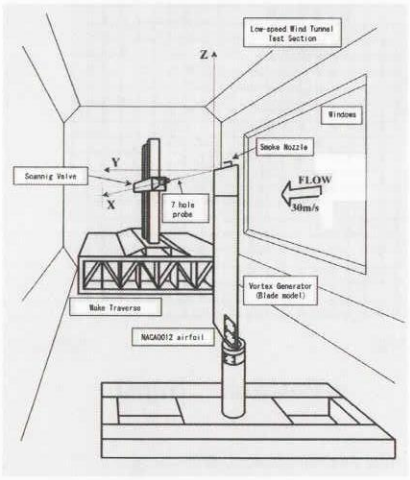

Figure A.1. Diagram of test section equipment system

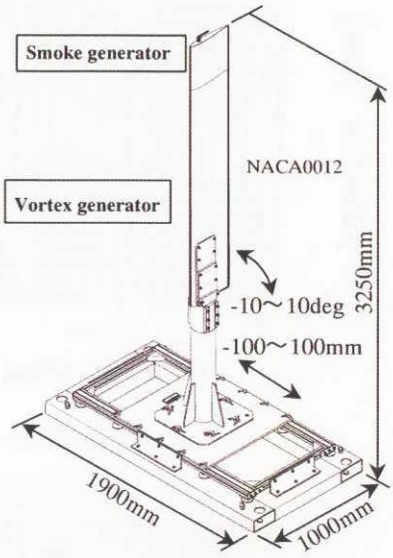

Figure A.3 Diagram of vortex/smoke generator

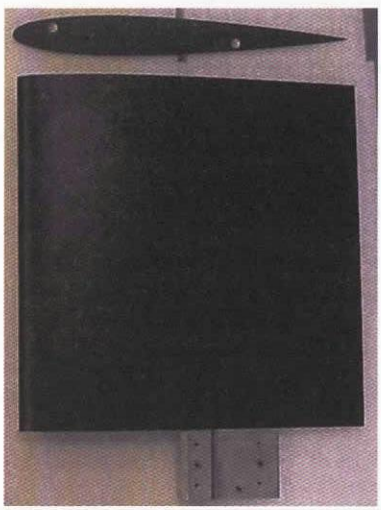

(a) square tip

Table A.1 Experimental test cases and results

Tip Shape	Angle of attack α [deg]	Maximum Velocity V_{max} [m/s]	Core Diameter d [mm]	Core Radius a [mm]	Circulation Γ	$(d/c)\times$ 100 [%]
Square	10	14.17	30	15	1.34	8.6
	5	6.46	20	10	0.41	5.7
Tapered	10	10.49	25	12.5	0.82	7.1
	5	4.78	15	7.5	0.22	4.3

The crossflow velocity, v and w, near the vortex core are obtained in the downstream section of 14-chord length behind the trailing edge of blade tip and the results are shown in Figure A.4 for two kinds of tip shape, square and tapered at the angle of attack of 5 and 10 degrees. Since NACA0012 airfoil is of symmetric shape, the cases for 10 degree and -10 degree angle of attack showed identically symmetrical vector plots. The vector plot shows that square tip at 10-deg angle of attack has maximum circumferential velocity measurement, i.e. strongest tip vortex. As the angle of attack increases, the core size of tip vortex and its strength increase. The measured and calculated results are described in Table A.1. The circulation of the vortex was defined with the maximum circumferential velocity and radius of vortex core as

$$\Gamma = 2\pi V_{\max} a \,.$$

The maximum circulation value was also shown for the square tip at 10-deg angle of attack, and the circulation increases as the angle of attack increases. The difference in circulation for between square and tapered tip shapes can be explained by the fact that tip vortex has its origin from the pressure difference between upper and lower surfaces of blade tip. Since the tapered tip shape has not only the short range for developing tip vortex but also small area in tip region, the square tip showed the stronger tip vortex in the way of core size and circulation.

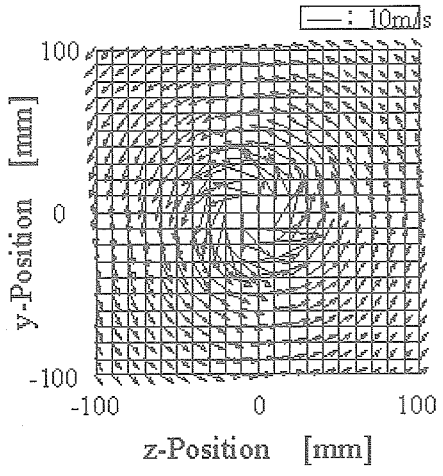

(a) rectangular, α=10deg

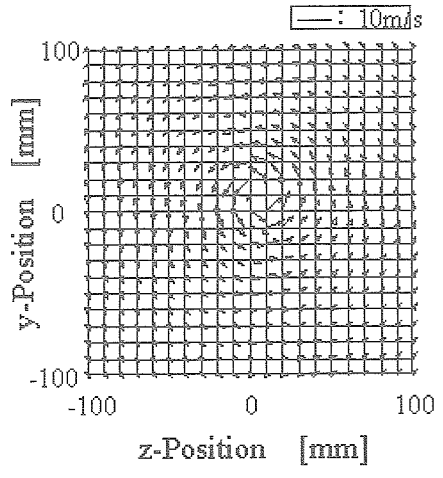

(b) rectangular, α=5deg

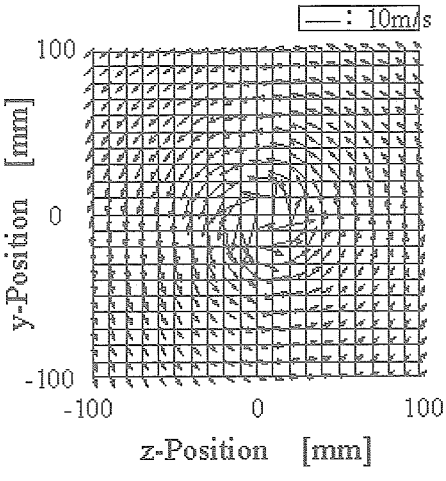

(c) tapered, α=10deg

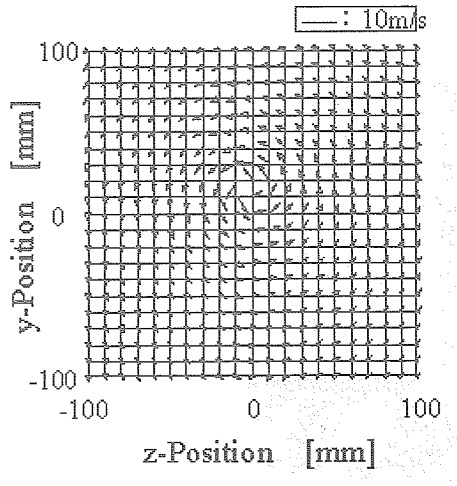

(d) tapered, α=5deg

Figure A.4 Vector plot for vertical velocity components, v and w (square and tapered, 10mm pitch, x/c=14)

Figure A.5 shows the circumferential velocity profiles of tip vortices measured at 14-chord length behind the blade for cases of the square and tapered tips at the angles of attack of 5 and 10 degrees. In this figure, velocities are non-dimensionalized by the maximum circumferential velocity and the distances from vortex center by the core radius of vortex. When the profiles are compared with some mathematical vortex models, experimental results are observed in good agreements with Scully model or Power-law model. Figure A.6 shows the formation of tip vortex visualized by Laser Light Sheet (LLS) technique using a smoke generator at the distance of 14-chord length behind the blade. The enlightened part of circular shape and the center of vortex core of the tip vortex are clearly seen by this LLS visualization technique.

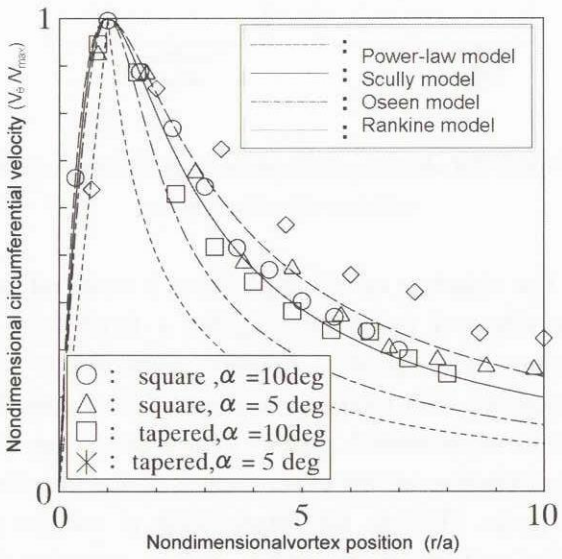

Figure A.5 Comparison of circumferential velocity profiles of tip vortices (rectangular, α=10deg ,x/c=5)

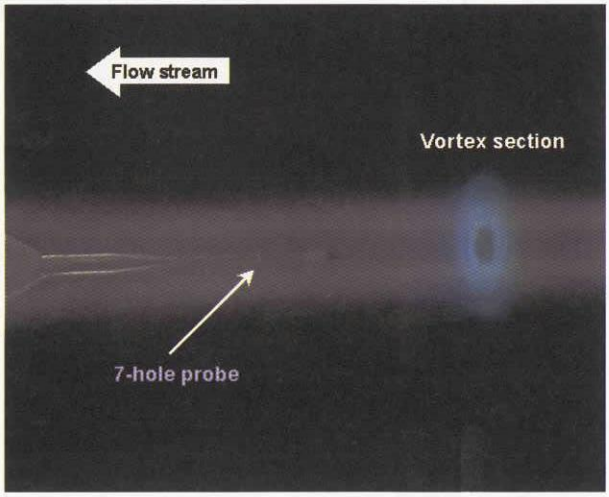

Figure A.6 Tip vortex visualization using LLS (rectangular type tip, $\alpha=10^o$)

APPENDIX B.

Experimental research for tip blowing in Kawada Industries, Inc[51,52]

The experiments are carried out in low speed wind tunnel of Kawada Industries, Inc. in Japan with 2.0m wide, 2.5m high, 15.0m long test section. It has single-stage axial blower directly connected to a driving motor with 12-bladed variable-pitch rotor of 4.0m diameter and 8-bladed stator installed downstream of the rotor. The capacity of motor is 220 kW with 0 ~ 360 RPM speed to produce the wind of 2m/s ~ 45m/s speeds.

The experiments are conducted with a blade model of 26mm-chord-length NACA0015 airfoil, which has 150mm span length and 5.77 aspect ratio. The free stream velocity was set to 20.0m/s, corresponding to a Reynolds number of 3.6×10^6. The mean flow quantities in the near wake region are measured with a 10mm diameter pitot tube. And tip vortex was measured at 1.3 chord length behind from the trailing edge using traverse with 110mm wide and 90mm high cross plane. The angle of attack was fixed at 10 degrees. The system diagram of wing-tip blowing experiment with fixed wing is shown in Figure B.1. The jet was injected at the tip by internal pressure P_w of blade chamber, P_w=0.05, 0.1, 0.2, 0.3, 0.4, 0.5Kg/cm^2. The injected compressed air can be non-dimensionalized with the injection velocity, V_j, sound velocity, a, injection Mach number, M_j, air properties, P_0, ρ_0,

T_0 , injected air properties, P, ρ, T, the ratio of specific heat, γ, and Gas constant, R.

The injection Mach number can be calculated by

$$M_j = \sqrt{\frac{2}{\gamma - 1}\left(\frac{P_0}{P_0 + P_w}\right)^{\frac{\gamma-1}{\gamma}} - 1}$$

The injection Mach number is M_j=0.3, 0.4, 0.5, 0.6, 0.7, 0.8

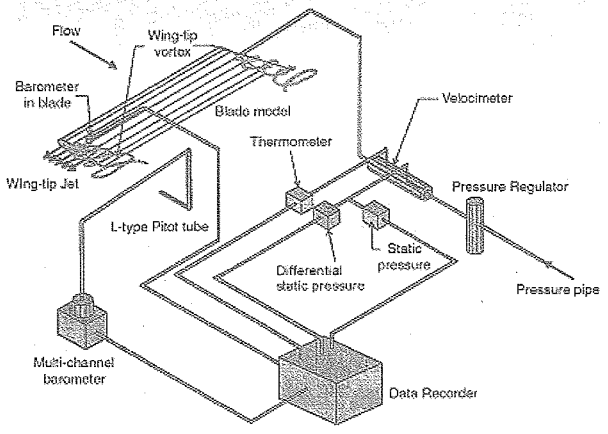

Figure B.1 System diagram of wing-tip blowing experiment with fixed wing

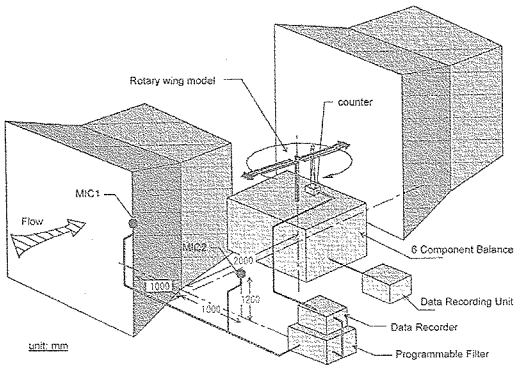

Figure B.2 System diagram of wing-tip blowing experiment with rotary wing

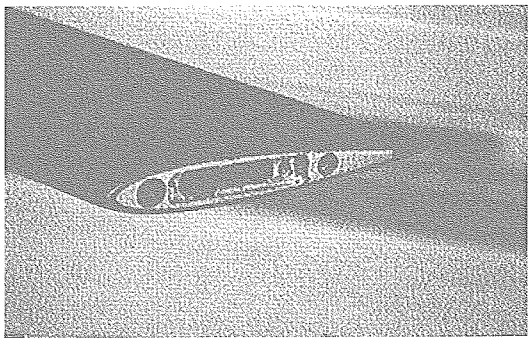

Figure B.3 jet blowing system

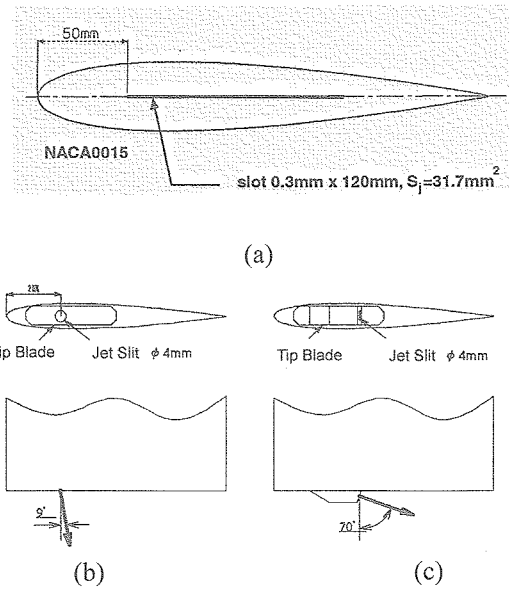

Figure B.4. Jet slit and diagram of jet blowing system with two injection angles

The objective of this experiment is to investigate the effect of tip-jet blowing for a fixed wing at various jet speeds. Another experiments are conducted with rotary wing model. The figure B.2 shows experimental system with rotary wing test. The objective of this experiment is to see the effect of tip-jet blowing for rotary wing at various jet speed and injection angles, and to compare the effect of rotation with fixed wing cases. The noise level was measured with microphone above the rotor.

Two kind of jet slit systems, one of which are shown in Figure B.3, are used to compare the effect of injection angles. Figure B.4 shows jet blowing system with two injection angles equals to 9 degrees and 70 degrees. The jet slit was to be concentrated with 4 mm diameter circle, and the noise reduction levels are calculated.

Figure B.5 shows the comparison of vortex position according to internal pressure for tip jet blowing. As internal pressure increases, which means the amount and velocity of jet blowing also increases, the center of vortex moves outward from the tip. Compared to the experimental data, numerical calculation of Euler compressible solver shows more distinct movement of vortex core to outward direction.

Figure B.6 shows the comparison of BVI peak of rotor according to various tip jet speeds when the tip rotation speed, V_{tip}=62.8m/s. As injection Mach number increases, the noise level decreases up to 3.6dB at specified experimental conditions. Figure B.7 shows comparison of BVI noise level reduction according to jet flow rate and injection angle. In this experiment, backward injection was found to be more effective to reduce the noise level compared to normal injection.

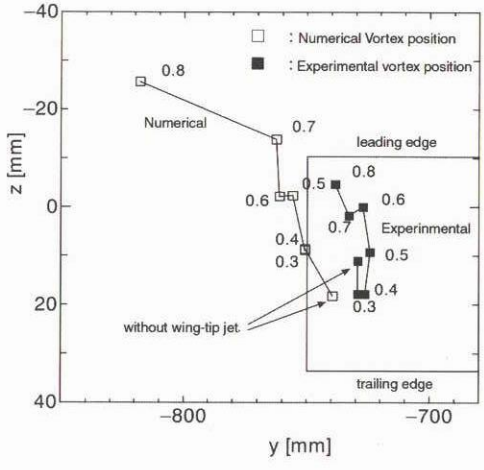

Figure B.5. Comparison of vortex position according to internal pressure for tip jet blowing

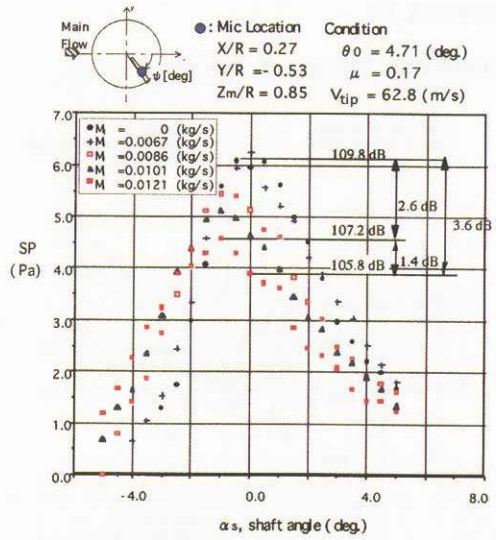

Figure B.6. Comparison of BVI peak of rotor according to tip jet speed (V_{tip}=62.8m/s)

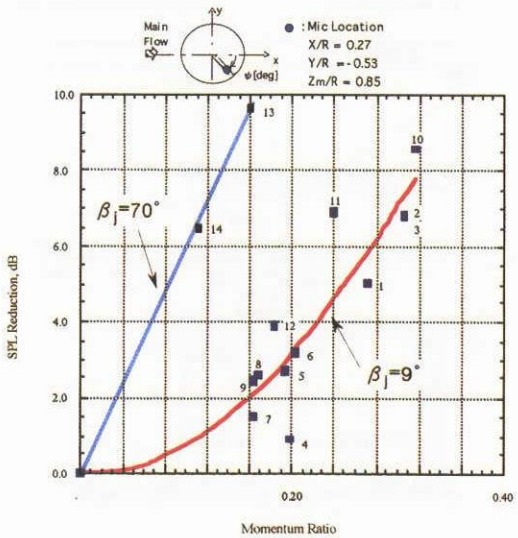

Data Point	M_{tip}	μ	θ_0 (deg.)	β_j
1	0.14	0.15	4.71	9°
2	0.14	0.16	4.71	9°
3	0.14	0.17	4.71	9°
4	0.14	0.15	8.3	9°
5	0.14	0.16	8.3	9°
6	0.14	0.17	8.3	9°
7	0.14	0.15	11.32	9°
8	0.14	0.16	11.32	9°
9	0.14	0.17	11.32	9°
10	0.14	0.18	5.0	9°
11	0.16	0.18	5.0	9°
12	0.19	0.18	5.0	9°
13	0.14	0.18	5.0	70°
14	0.19	0.18	5.0	70°

Figure B.7 Comparison of BVI noise level reduction according to jet flow rate and injection angle

APPENDIX C.

Experimental System in DNW

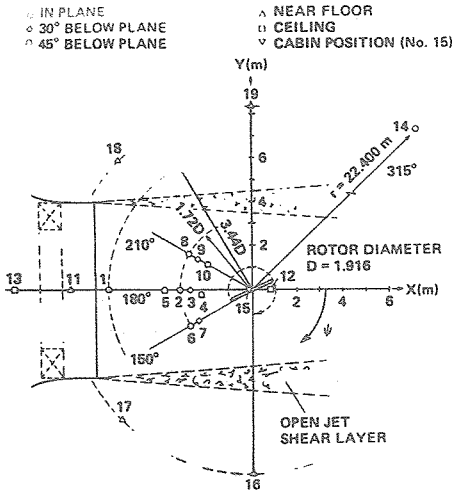

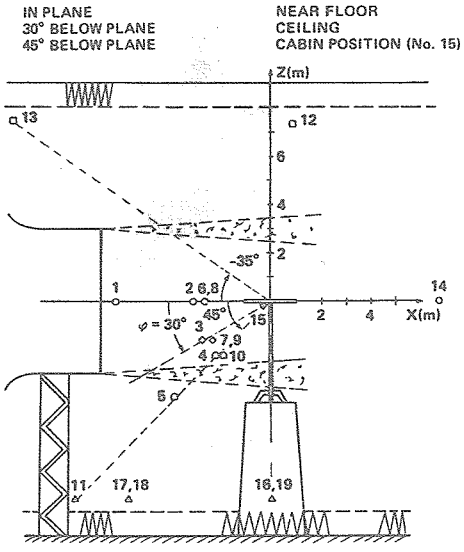

Ref. Boxwell, D.A., Schimitz, F.H., Splettstoesser, W.R. and Schults, K.J., "Helicopter model rotor-blade vortex interaction impulsive noise: scalability and parametric variations", Journal of American Helicopter Society, Vol.32, No.1, pp.3-12

ACKNOWLEDGEMENT

I would like to thanks to the assistances and advices from Akio Ochi and Natsuki Kondo in ATIC (Advanced Technology Institute of Commuter-helicopter, Ltd.). Also I thanks to Noriko Yamamoto, Uichi Nishizawa, Masataka Shirai, Naofumi Suenaga, Seiichi Kawada and Ayumu Yamaguchi for their kindness and heartful help.

This research work has been partially supported by JKF Research Program for Researcher and Technologist during author's staying in National Aerospace Laboratory, Tokyo, Japan from October of 1999 to October of 2000.

JAXA Research and Development Report
(JAXA-RR-04-013E)

Data of Issue: Aug 31,2004

Edited and Published By:
Japan Aerospace Exploration Agency
7-44-1 Jindaiji-higashimachi,Chofu-shi,
Tokyo 182-8522 Japan

Printed by:
NORTH ISLAND CO., Ltd.
4-1-9 hibarigaokakita, Nishitokyo-shi, Tokyo 202-0002 Japan

Japan Aerospace Exploration Agency